A +CG flash caused by a sequence of bidirectional leaders that served to form a ground-reaching branch of a pre-existing horizontal channel

Bin Wu[1,2], Weitao Lyu[1,2], Qi Qi[1,2], Ying Ma[1,2], Lyuwen Chen[3], Ruijiao Jiang[1,2,5], Yanan Zhu[4] and Vladimir A. Rakov[5]

[1]State Key Laboratory of Severe Weather, Chinese Academy of Meteorological Sciences, Beijing 100081, China

[2]Laboratory of Lightning Physics and Protection Engineering, Chinese Academy of Meteorological Sciences, Beijing 100081, China

[3]Institute of Tropical and Marine Meteorology, China Meteorological Administration, Guangzhou 510080, China

[4]Earth System Science Center, University of Alabama in Huntsville, Huntsville, Alabama, USA

[5]Department of Electrical and Computer Engineering, University of Florida, Gainesville, Florida, USA

Corresponding author: Weitao Lyu (wtlu@ustc.edu)

Key Points:

- Bidirectional leaders developed below a previously formed horizontal channel and served to form a new positive branch that attached to the ground

- Connection of the negative (upper) end of each bidirectional leader to the horizontal channel resulted in abrupt elongation of the positive (lower) end

- Flickering streamer-like filaments (needles) extended sideways from the horizontal channel in response to the injection of negative charge associated with the +CG

Abstract

High-speed video and electric field change data were used to analyze the initiation and propagation of four predominantly vertical bidirectional leaders making connection to a predominantly horizontal channel previously formed aloft. The four bidirectional leaders sequentially developed along the same path and served to form a positive branch of the horizontal in-cloud channel, which became a downward positive leader producing a 135-kA positive cloud-to-ground (+CG) return stroke. The positive (lower) end of each bidirectional leader elongated abruptly at the time of connection of the negative (upper) end to the pre-existing channel aloft. Thirty-six negative streamer-like filaments (resembling recently reported "needles") extended sideways over ~110 to 740 m from the pre-existing horizontal channel at speeds of ~0.5 to 1.9×10^7 m/s, in response to the injection of negative charge associated with the +CG.

Plain Language Summary

This paper presents high-speed video records that show how a sequence of predominantly vertical bidirectional leaders can lead to formation of a positive branch of the previously formed predominantly horizontal channel aloft, with this branch eventually making contact with the ground and initiating a positive cloud-to-ground (+CG) return stroke. Additionally, the recently discovered "needles" have been optically imaged and characterized. Observations were performed at the Tall-Object Lightning Observatory in Guangzhou (TOLOG), China. This study helps to improve our understanding of one of the initiation mechanisms of +CG flashes that involves downward branching of in-cloud lightning channels.

1. Introduction

One of the most challenging issues in the physics of lightning is the interpretation of the initiation mechanisms of positive cloud-to-ground (+CG) discharges. According to Rakov and Uman (2003), +CG can be just a byproduct of a cloud discharge. Recently, Nag and Rakov (2012) described 6 conceptual cloud charge configurations and scenarios that were observed or hypothesized to give rise to positive lightning, with one of the scenarios being a positive branch of an in-cloud discharge channel (see Section 2.6 and Figure 1f in their paper). High-speed

video images of such flashes are found in the works of Kong et al. (2008) and Saba et al. (2008, 2009). However, as of today there are no documented cases showing the process of such branch formation. Observations show that branches of in-cloud channels can involve a sequence of bidirectional leaders (Warner et al., 2016; Yuan et al., 2019) that, in effect, can facilitate connection of a channel aloft to ground (Tran and Rakov 2016).

High-speed video and VHF observations are two widely used methods to analyze the dynamics of leader initiation and propagation. However, the relatively strong negative breakdown VHF signals associated with the negative end of bidirectional leaders, tend to mask the relatively weak positive breakdown VHF signals associated with the simultaneously propagating positive end (Shao et al., 1999). Consequently, it is often difficult for VHF imaging systems to detect the positive end of bidirectional leaders. Bidirectional propagation of leaders can be detected (imaged) with high-speed video cameras that have yielded important results published by Jiang et al. (2014), Montanyà et al. (2015), Takamatsu et al. (2015), Kostinskiy et al. (2015), Warner et al. (2016), Tran and Rakov (2016), Yuan et al. (2019), and Wu et al. (2019a). In particular, Montanyà et al. (2015) reported a recording of bidirectional intracloud lightning (IC) initiation in virgin air at ~11,000 frames per second (fps). Tran and Rakov (2016) observed that the negative end of a bidirectional leader contacted ground and produce a negative cloud-to-ground (-CG) return stroke. However, bidirectional leaders often develop completely inside the cloud, which makes their optical imaging difficult. Only a few quality recordings are presently available. As a result, the details of dynamics of bidirectional leaders resulting in the formation of a ground-reaching leader are still not completely understood.

Positive lightning discharges account for about 10% of all CG discharges (e.g., Rakov, 2003), so positive lightning discharges are considerably less studied and understood than their negative counterparts. Furthermore, most of the existing optical observations of +CG flashes can only yield some characteristics after the leader emerges from the cloud. To the best of our knowledge, to date, there are no optical records of the complete dynamics of +CG flashes. High-speed video observations reviewed above confirm that in-cloud channels giving rise to

80   CG discharges can be produced by bidirectional leaders. However, details of the formation of a

81   downward positively charged ground-reaching branch have not been reported before.

82   In this paper, we present optical and electric field observations of the formation process

83   of ground-reaching positive branch of an in-cloud channel initiating a +CG return stroke. The

84   observations were performed at the Tall-Object Lightning Observatory in Guangzhou

85   (TOLOG), China. The dynamics of all stages of the +CG flash are examined and discussed in

86   detail. Among other things, our records show flickering streamer-like filaments (resembling

87   recently reported "needles" observed with RF imaging systems by Hare et al., 2019 and Pu and

88   Cummer, 2019 and optically by Saba et al., 2020) extending sideways from the horizontal

89   in-cloud channel energized by the +CG.

90   **2. Instrumentation and Data**

91   The TOLOG (Lu et al., 2012, 2013; Qi et al., 2019; Wu et al., 2019b) is located on the

92   roof of an approximately 100-m-high building of the Guangdong Meteorological Bureau. The

93   optical instrumentation used in this study consisted of a lightning channel imager (LCI) and

94   two high-speed video cameras (HC-1 and HC-2) operating at different framing rates

95   (20,000-fps and 50,000-fps, respectively). The focal lengths of HC-1 and HC-2 were 14 and 20

96   mm, respectively, and the record lengths were 50 and 20 ms, respectively. The corresponding

97   pre-trigger times were 25, and 10 ms and the corresponding spatial resolutions were 1024

98   pixels $\times$ 1024 pixels and 512 pixels $\times$ 272 pixels. The framing rate and focal length of the

99   lightning channel imager (LCI) were 50-fps and 5 mm, respectively. The record length,

100   corresponding pre-trigger time and corresponding spatial resolution of LCI were 2 s, 500 ms,

101   and 780 pixels $\times$ 582 pixels, respectively.

102   Electric field changes were measured using a set of fast and slow antenna systems. The

103   time constants of the fast and slow antennas were 1 ms and 6 s, respectively, and the sampling

104   rate of the two field measuring systems was 10 MHz. The record lengths and pre-trigger times

105   of the fast and slow antenna systems were 1 s and 100 ms, respectively. The measurement

106   ranges of the fast and slow antenna systems were ±100 kV/m and ±200 kV/m, respectively, and

107   the vertical resolution of each of them was 12-bit.

Signals from one of the eight channels of the Lightning Attachment Process Observation System (LAPOS, Wang et al., 2011) recorded by a digital oscilloscope was used for triggering the cameras and the field measuring systems. Each trigger event was time-stamped using a GPS clock with accuracy of 30 ns. In addition, we obtained information on the location of lightning channel ground termination point, the time of return stroke, and the estimated peak current of the +CG return stroke from the Guangdong-Hong Kong-Macao Lightning Location System (GHMLLS).

The +CG flash (denoted F17149) considered here contained a single stroke. The GHMLLS reported that stroke to be located approximately 17 km from the observation station and estimated its peak current to be approximately +135 kA. In this paper, we analyzed the characteristics of bidirectional leaders involved in the initiation and development of the +CG. Additionally, we examined streamer-like filaments extending sideways from the horizontal in-cloud channel energized by the +CG. All the lengths and speeds presented are two-dimensional (2-D) and estimated based on the distance between the +CG ground termination point and TOLOG. All times are relative to the onset of the return stroke of the +CG flash. The atmospheric electricity sign convention was used in this study.

3. Data Presentation and Results

The LCI operated at 50-fps (20-ms interframe interval) with a recording time of 2 second and completely recorded the entire +CG lightning flash (see Movie S1 in the supporting information). Figure 1 shows 7 consecutive LCI images, with an exposure time of approximately 20 ms each, with the time stamp on each image being the end of exposure time relative to the return-stroke onset. No luminous channels were seen for about 500 ms in the LCI record prior to the -79-ms frame. A short floating channel appeared in the -79-ms frame (see the smaller rectangular box and its expansion in Figure 1b). The floating channel became visible during the -99 to -79 ms time interval and then clearly exhibited bidirectional development extending horizontally over about 15 km from -79 to -59 ms (see Figure 1c).

In the next two frames (see Figures 1d and 1e), the bidirectional leader channel did not exhibit further extension, but its brightness increased from -59 to -39 ms and then decreased from -39 to -19 ms. The predominantly vertical (positive leader/return stroke sequence)

channel connecting the previously formed predominantly horizontal channel with the ground is seen in Figure 1f. However, due to the insufficient temporal resolution of LCI, the dynamics of that connection is not resolved in Figure 1. Note that the junction point between the positive leader/return stroke channel and the previously formed horizontal channel was near the right end of the initial horizontal channel segment seen in Figure 1b (see vertical broken line passing through Figures 1b, 1d, and 1f).

We now present our records obtained using the high-speed video camera (HC-1) operating at 20,000-fps (50-μs interframe interval) with a recording time of 50 ms. These records (see Movie S2 in the supporting information) clearly show that the downward positive leader evolved from a sequence of four bidirectional leaders that developed along the same, predominantly vertical path below the predominantly horizontal channel whose development is seen in Figure 1. Figure 2a shows a composite image of 40 selected HC-1 frames before the onset of the +CG return stroke. These frames were selected to best display the geometry of the horizontal channel aloft and the following four bidirectional leaders, the last of which completed the formation of the downward branch of the horizontal channel, which forged its way to ground and produced the +CG return stroke.

Figure 2b shows the image brightness record along with the fast and slow antenna system electric field changes. The bipolar pulses (labeled BPs) in the fast electric field change record (labeled FA in Figure 2b) that occurred about 60 ms prior to the return stroke (labeled +RS) corresponds to the full (about 15 km) extension of the horizontal channel seen in Figure 1c (-59-ms, end of exposure time). Between -50 and -40 ms, K change type signatures are seen in the fast electric field change record. Note that between -59 and -39 ms, the brightness of the horizontal channel increased (see Figure 1d). It follows from Figure 1 that no vertical channel was formed before -19 ms. However, at that time the slow electric field change record, labeled SA in Figure 2, shows significant positive (opposite to the +RS) field deflection, which is indicative of the motion of positive charge toward the observer. In fact, the positive field deflection started at about -60 ms, and the slow field change between -60 ms and 0 is characteristic of downward positive leader signature, although the downward extension apparently did not start until -19 ms or so. It is likely that the positive charge motion toward the

166 observation station between -60 and -19 ms is indicative of the entire horizontal channel being

167 charged positively. Electric field signatures of the beginning and the intensification of this

168 latter process in the FA record are marked as "BPs" (bipolar pulses) and "K changes",
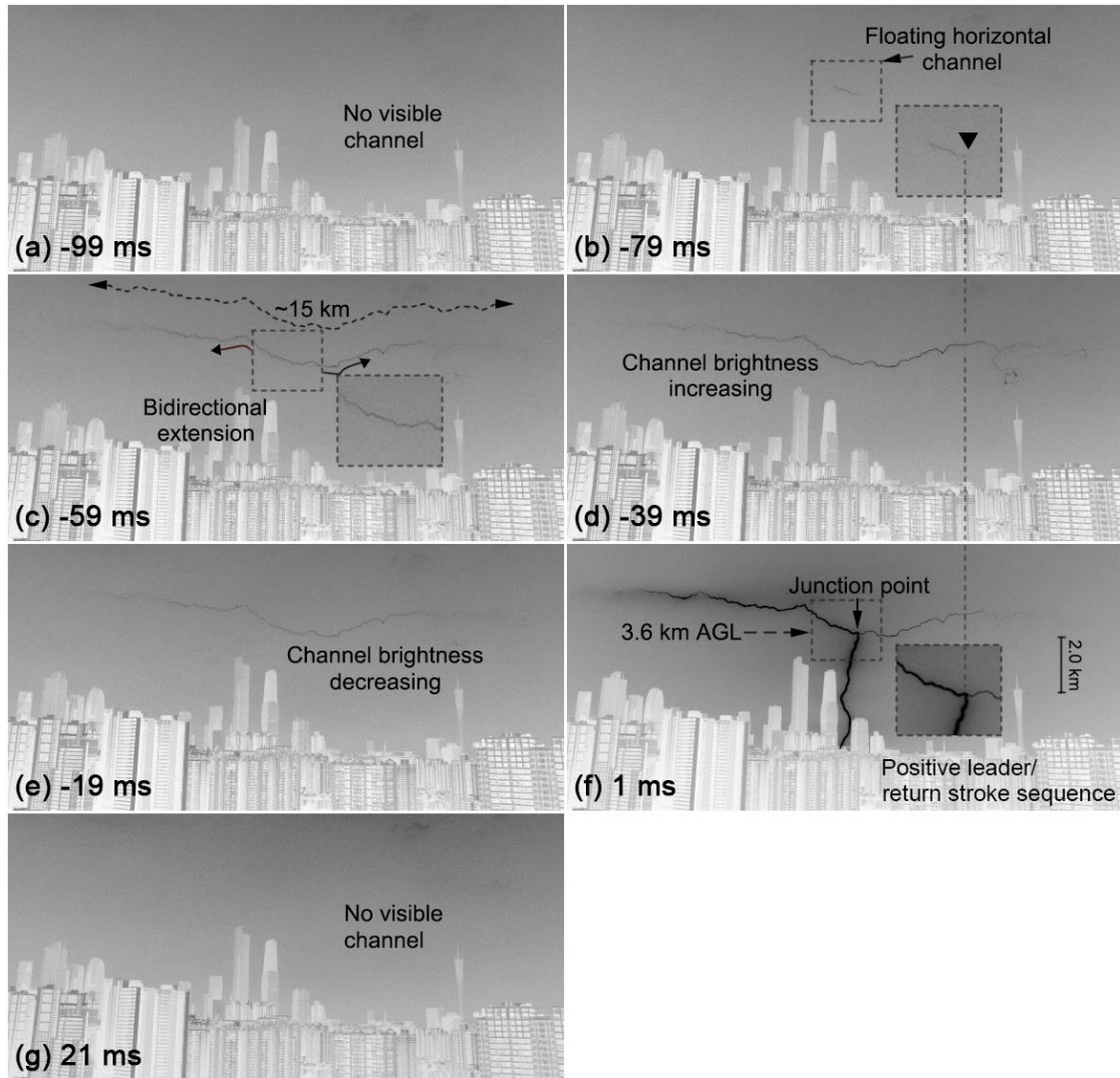
169 respectively, in Figure 2b.

170

171 **Figure 1.** Seven consecutive images obtained using the lightning channel imager (LCI)

172 operating at 50 frames per second (20-ms interframe interval). The time stamp on each image

173 corresponds to the end of exposure time, adjusted based on synchronized images from HC-1.

174 The images were cropped, inverted, and contrast enhanced. Portions of images in smaller

175 broken-line boxes are shown enlarged in (b), (c), and (f). Small inverted triangle in (b)

176 indicates the inferred origination point of the predominantly horizontal channel, whose

177 development is seen in (b) and (c).

178   Four bidirectional leaders (BL_1-BL_4) associated with formation of downward positive

179   leader occurred approximately 20, 12, 9, and 4 ms before the onset of the +CG return stroke

180   (see the brightness trace in Figure 2b). BL_1 to BL_4 produced no pronounced electric field

181   changes (see the FA and SA traces in Figure 2b), because they were relatively far

182   (approximately 17 km) from observation station. The upper end of each bidirectional leader

183   extended upward (this extension is imaged for BL_1, BL_3, and BL_4 and inferred for BL_2) and

184   contacted the previously formed horizontal channel, forming a downward branch of the

185   horizontal channel that eventually made contact with the ground. The height of the junction

186   point was approximately 3.6 km above ground level (AGL). The polarity of charge transfer to

187   ground was positive, based on the negative electric field change at t = 0 (see +RS in Figure 2b).

188   Consequently, the lower end of each bidirectional leader must have been positive, with the

189   upper end being negative and the horizontal channel aloft (at least near the junction point)

190   being positive.

191   During the +CG return stroke stage, the left part of the horizontal channel was much

192   brighter than the right one (see Movies S2 and S3 in the supporting information), which

193   suggests that positive charge was supplied to the vertical channel to ground mostly by the left

194   part of the horizontal channel. However, the brightness of the right part also increased during

195   the return-stroke stage and, hence, it also participated in delivering positive charge to the

196   junction point (in other words, the negative charge injected by the +CG return stroke into the

197   junction point moved both to the left and to the right along the horizontal channel). Further,

198   during BL_1-BL_4 (approximately -20 ms to 0), the electric field was dominated by the motion of

199   positive charge toward the observation station (see the SA trace in Figure 2b), which indicates

200   that the middle part of the floating horizontal channel (near the prospective junction point) was

201   positive. There were other bidirectional leaders that served to form short branches in the left

202   part of the horizontal channel (see Bidirectional leaders appeared on the left part of the

203   horizontal channel in Figure 2a). Those are not further discussed in this paper.
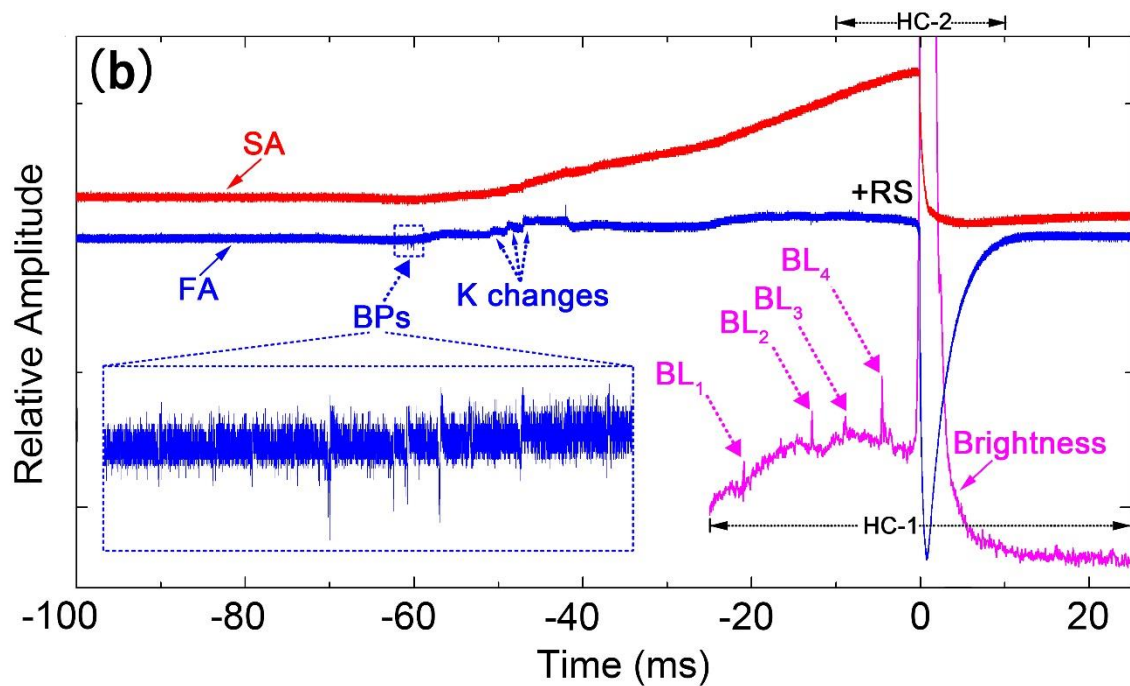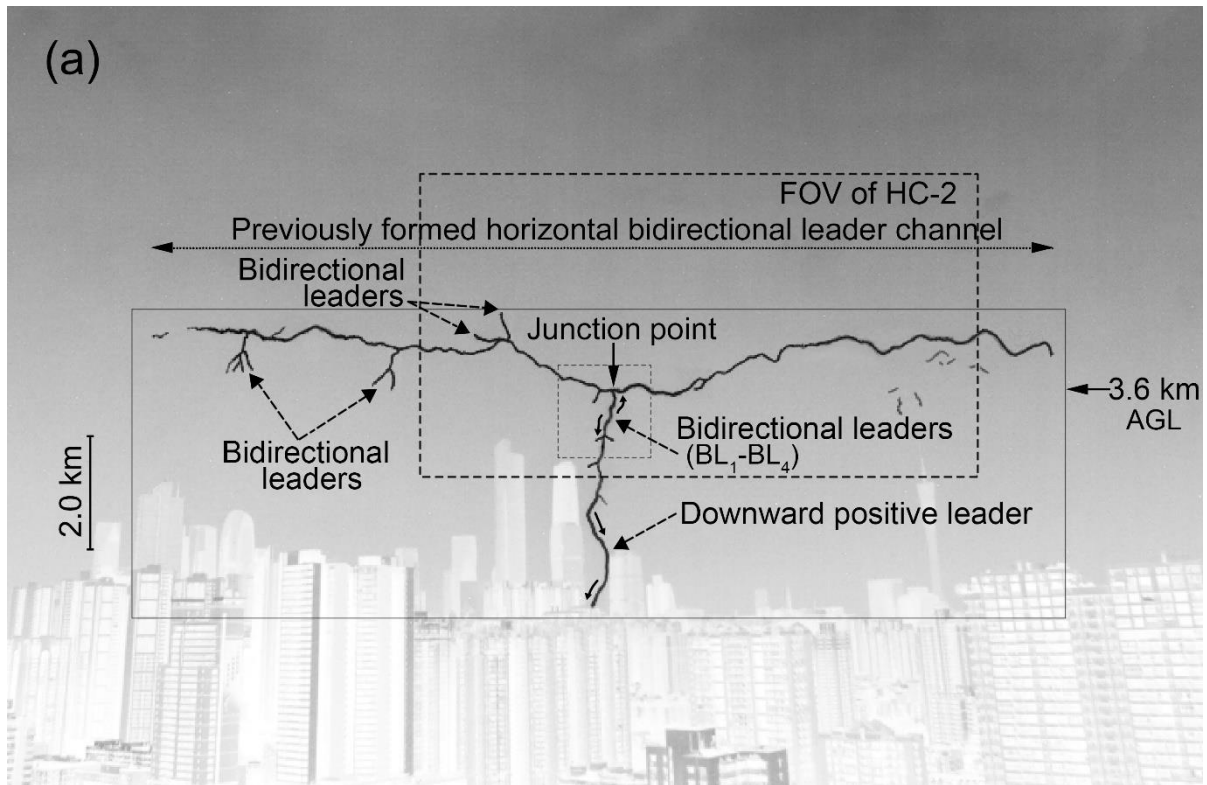
204

205

Figure 2. (a) Composite image of 40 selected frames (from −25 to −0.05 ms) obtained using HC-1 operating at 20,000 frames per second (50-μs interframe interval), showing the geometry of downward positive leader channel to ground (formed via a sequence of four bidirectional leaders, which connected to the previously formed horizontal channel aloft). (b) Synchronized optical image brightness (the sum of gray values of all pixels in each HC-1 image) within -25 to

211   25 ms time window, and fast (FA) and slow (SA) electric field change records (from -100 to 25

212   ms). The image shown in (a) was cropped, inverted, and contrast enhanced. The curved arrows

213   indicate the observed directions of channel extension. Single-frame and composite HC-1

214   images of the solid-line rectangular area seen in (a) that show the salient features of the

215   discharge development after the formation of the horizontal channel aloft are presented in

216   Figures 3a-3n. The dashed-line rectangular box in (a) shows the field of view (FOV) of HC-2.

217   The time window corresponding to images recorded by HC-2 is from -10 to 10 ms. The larger

218   dashed-line rectangular box in (b) is an expanded view for the smaller dashed-line rectangular

219   box labeled BPs. Labels BL_1–BL_4 are used to mark four bidirectional leaders examined in

220   detail. AGL = above ground level; +RS = positive return stroke; SA = slow antenna; FA = fast

221   antenna; BPs = bipolar pulses.

222   Figure 3 shows key processes seen in the HC-1 records inside the solid-line rectangular

223   box in Figure 2a after the formation of horizontal channel aloft. Four bidirectional leaders

224   (BL_1-BL_4) sequentially initiated and developed along the same predominantly vertical path

225   below the previously formed horizontal channel. The positive (lower) end of each following

226   bidirectional leader was closer to the ground than that of the preceding one (see Figures 3b, 3d,

227   3f, and 3h). The lengths of four bidirectional leaders (BL_1-BL_4) progressively increased by

228   approximately 190 m from BL_1 to BL_2, 250 m from BL_2 to BL_3, and 370 m from BL_3 to BL_4.

229   The sequence of four bidirectional leaders (BL_1-BL_4) served to form a new downward positive

230   branch of the horizontal channel. The newly formed downward branch gradually decayed

231   within ~0.3 ms (see Figures 3h and 3i) and became undetectable (see Figure 3j). Then this

232   branch reilluminated (see Figure 3k) and continued extending toward ground. Comparing the

233   positions of its tip in Figures 3h and 3k, we found that the downward branch elongated by ~160

234   m, while its luminosity was undetectable for ~0.45 ms (see Figure 3j).
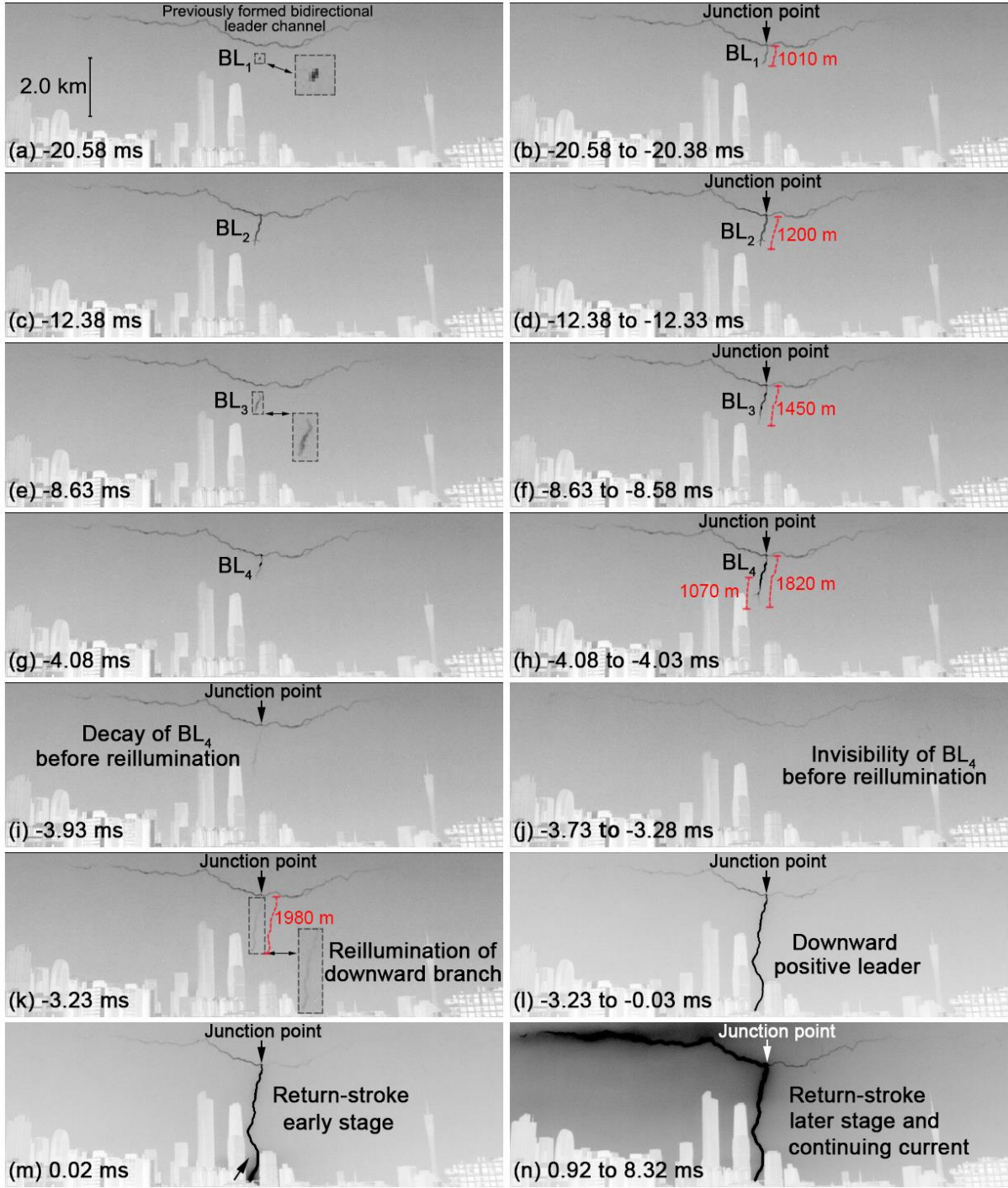
Figure 3. Key processes seen in HC-1 (50-μs interframe interval) records inside the solid-line rectangular box shown in Figure 2a after the formation of horizontal channel aloft: (a) first image of the first bidirectional leader (BL$_1$) channel, (b) composite image showing maximum extent of the BL$_1$ channel, (c) first image of the second bidirectional leader (BL$_2$) channel, (d) composite image showing maximum extent of the BL$_2$ channel, (e) first image of the third bidirectional leader (BL$_3$) channel, (f) composite image showing maximum extent of the BL$_3$

11

channel, (g) first image of the fourth bidirectional leader (BL$_4$) channel, (h) composite image

showing maximum extent of the BL$_4$ channel, (i) image of decaying fourth bidirectional leader

(BL$_4$) channel (downward branch), (j) image in which the downward branch is undetectable,

(k) first image showing reillumination of the downward branch formed via the sequence of BL$_1$

to BL$_4$, (l) composite image showing the fully formed downward positive leader, (m) image of

the return-stroke early stage, (n) composite image showing the return-stroke later stage and

continuing current. Time labels correspond to the end of frame exposure times measured with

respect to the return stroke onset. Red dashed lines are used to show the lengths of channel

segments of BL$_1$-BL$_4$ and of the resultant downward branch. Images from 0.02 to 0.92 ms are

overexposed.

Then the re-illuminated downward branch evolved into a fully developed downward

positive leader (see Figure 3l), attached to the ground, and initiated a +CG return stroke (see

Figure 3m). Based on (not shown here) consecutive frames of HC-1 and HC-2 (obtained from

Movies S2 and S3 in the supporting information), the entire discharge channel (including the

vertical channel to ground and both left and right parts of the horizontal channel) exhibited

light blooming during the +CG return stroke, but the brightness increase of the left part of the

horizontal channel was significantly larger than that of the right part. During the later stage of

return stroke and continuing current, the left part maintained elevated brightness, while the

right part just returned to the brightness level seen before the return stroke (see Figure 3n).

Therefore, as noted earlier, it appears that mostly the left part was active during the positive

leader/return stroke sequence, although the right part also contributed some current,

particularly during the continuing current stage, as seen in Figure 7.

Figures 4a-4h show 8 consecutive images of BL$_1$, and 6 consecutive images of BL$_2$ are

shown in Figures 4i-4n. BL$_1$ initiated at a height of 3.1 km AGL and at a distance of ~500 m

from the horizontal channel above it. Its bidirectional extension is clearly seen in Figures 4b

and 4c, although its lower end became undetectable in Figure 4d. By overlaying the BL$_1$

channels in Figures 4c and 4d, we found that the two channels had a common part. It is possible

that the lower part of the BL$_1$ channel in Figures 4d decayed, while its upper part survived and

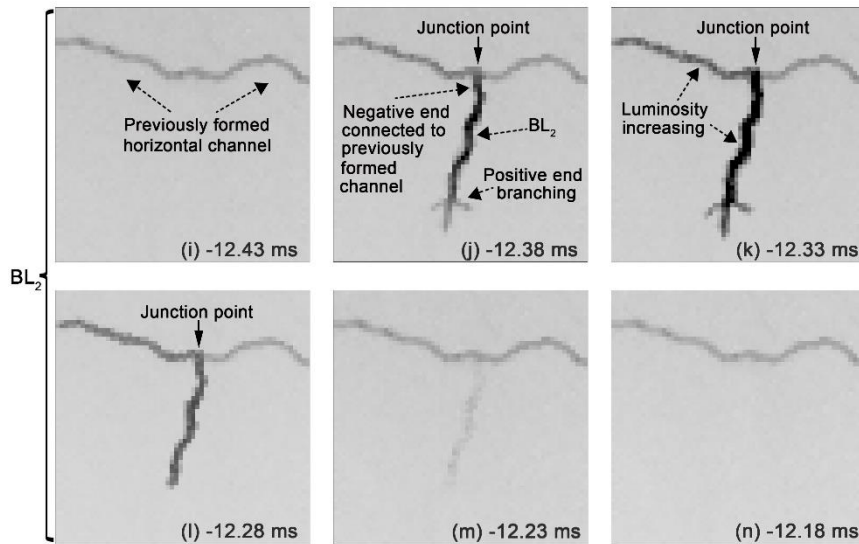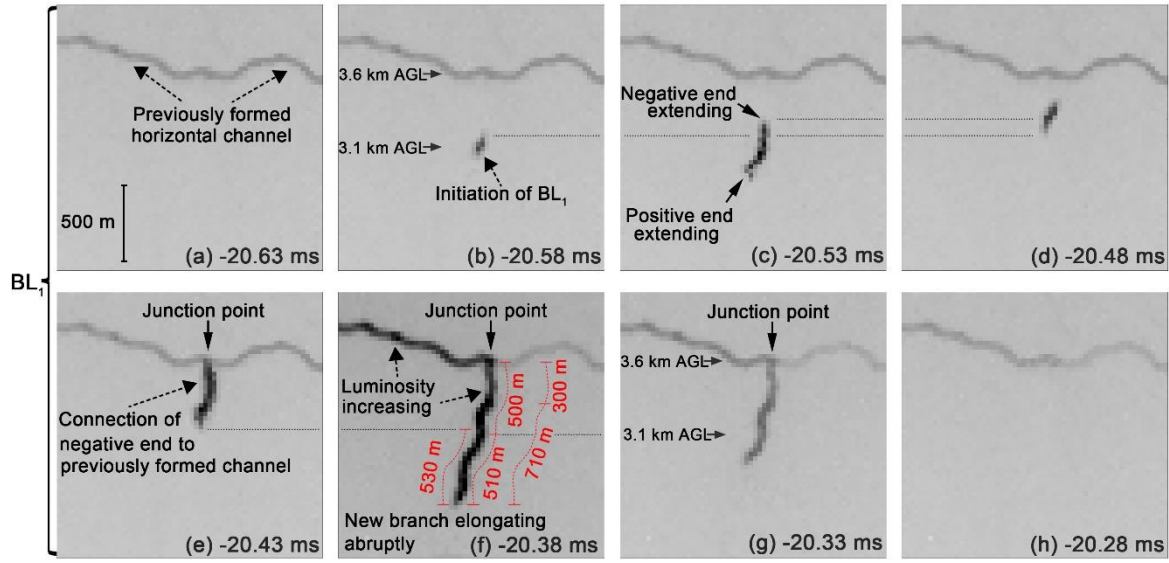eventually made connection to the horizontal channel as seen in Figure 4e.

271

272

Figure 4. (a-h) Eight consecutive HC-1 (50-µs interframe interval) images of the evolution of first bidirectional leader (BL$_1$) and (i-n) six consecutive HC-1 images of the second bidirectional leader (BL$_2$) within the small dotted-line rectangular box shown in Figure 2a. The solid-line rectangular box labeled 3 in panel (d) is a superposition of boxes labeled 1 and 2 in panels (c) and (d), respectively. Each image was inverted and contrast enhanced. The time stamp given on each image is the end of the exposure time. Red dashed lines are used to show the lengths of negative and positive ends of BL$_1$. For BL$_2$, no upward extension was detected, probably due to insufficient time resolution of the camera or low (undetectable) brightness of BL$_2$ channel in (i). BL = bidirectional leader; AGL = above ground level.

13

282   After the connection, the luminosity of BL_1 and the left part of the horizontal channel

283 increased significantly, while the luminosity of its right part diminished (see Figure 4f). The

284 connection was also associated with elongation of BL_1 channel by approximately 530 m (see

285 Figure 4f), retracing the previously formed but decayed BL_1 channel seen in Figure 4c. The

286 effective 2-D elongation speed was approximately 1.1×10^7 m/s. Then the new positive branch

287 formed by BL_1 gradually decayed (see Figure 4g) and became undetectable in Figure 4h.

288   It is unknown whether the polarity reversal (neutral) point of BL_1 was stationary at 3.1

289 km AGL (see Figure 4b) or moved up as its lower part decayed (see Figure 4d). In the former

290 case, the extension of the negative end was approximately 500 m (see Figure 4f), which is

291 about the same as the extension of the positive end (approximately 510 m). In the latter case,

292 the extension of the negative end was approximately 300 m (see Figure 4f), with the positive

293 end extension being approximately 710 m.

294   Figure 4i shows the frame just preceding the occurrence of BL_2 (7.85 ms after the decay

295 of BL_1). In its first image (Figure 2j), BL_2 appears to be already connected to the horizontal

296 channel aloft, which can be due to insufficient temporal resolution of the camera or low

297 (undetectable) brightness of BL_2 channel in Figure 4i. BL_2 followed the decayed channel of

298 BL_1 (compare Figures 4j and 4f). Further, the brightness of the new branch formed by BL_2 and

299 the left part of the horizontal channel in Figure 4k increased, similar to Figure 4f. This

300 similarity makes us believe that event BL_2 was indeed a bidirectional leader. Note branching at

301 the lower (positive) end of the BL_2 channel (see Figures 4j and 4k), which is usually considered

302 as evidence of leader extension in virgin air (e.g., Tran and Rakov 2016).

303   Unlike BL_1 and BL_2, BL_3 and BL_4 were recorded, with a better time resolution (20-µs

304 interframe interval), by HC-2 (see Movie S3 in the supporting information), within -10 to 10

305 ms time windows shown in Figure 2b. The dynamics of BL_3 and BL_4 are shown in Figure 5.

306 Figures 5a-5f show 6 consecutive images of BL_3, which occurred approximately 3.5 ms after

307 BL_2. The initiation height of BL_3 (2.9 km AGL and 700 m below the horizontal channel) was

308 approximately 200 m lower than that of BL_1. BL_3 initiated and extended bidirectionally in the

309 remnants of the decayed channel of BL_2. Similar to BL_1, brightness of the left part of the

310 horizontal channel and that of BL_3 itself increased after the connection of the negative (upper)

14

311   end of BL_3 to the horizontal channel (see Figures 5e and 4f). However, in contrast to BL_1, BL_3

312   was extending without interruption until its connection to the horizontal channel (see Figures
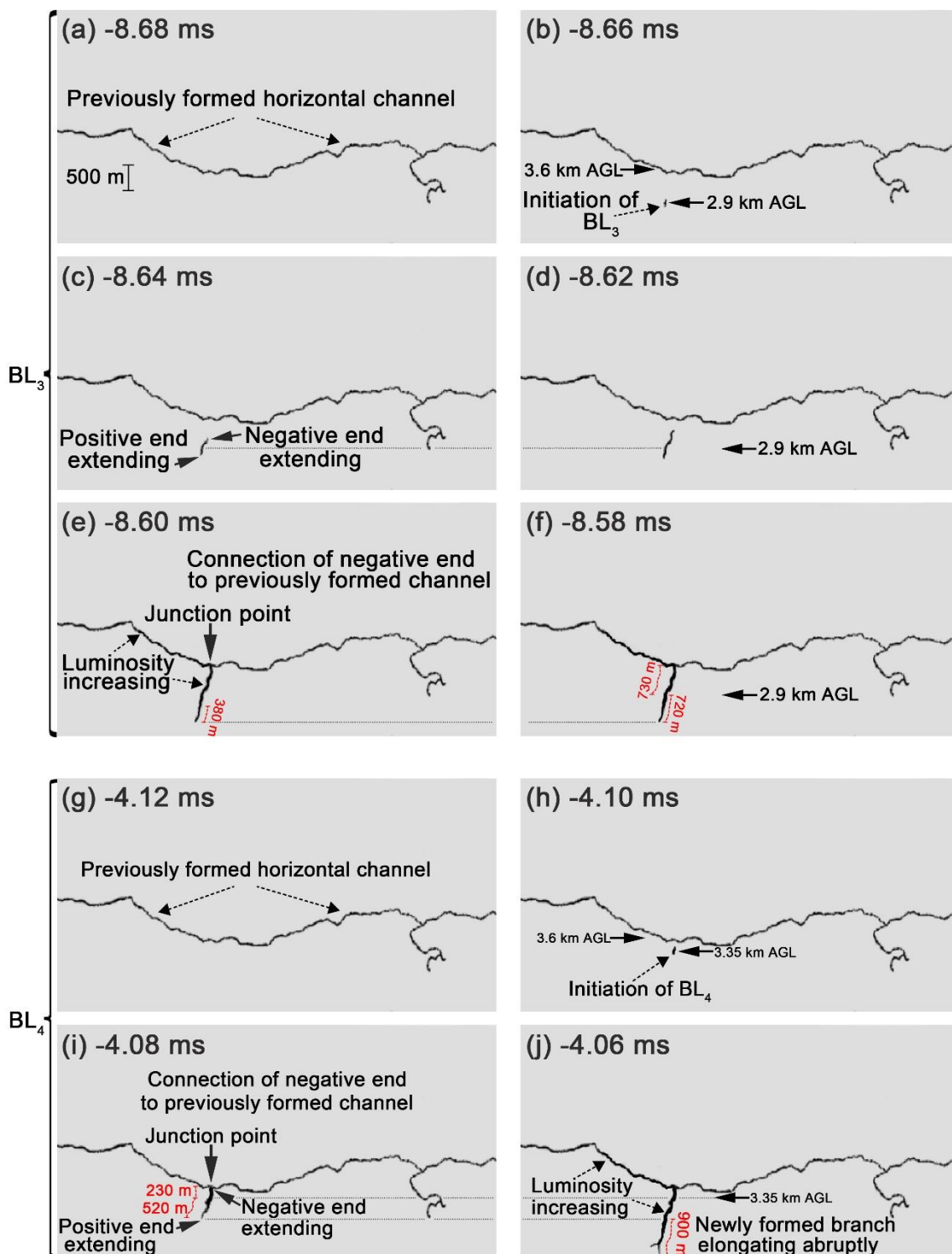
313   5c-5e).

314

315

Figure 5. (a-f) Six consecutive HC-2 (20-μs interframe interval) images of BL_3 and (g-j) four consecutive HC-2 images of BL_4. The images were background removed, inverted, and contrast enhanced. The time stamp given on each image is the end of the exposure time. The dashed-line rectangular box in Figure 2a shows the FOV of HC-2. Red dashed lines are used to show the lengths of channel segments of BL_3 and BL_4. BL = bidirectional leader; AGL = above ground level.

In Figure 5e, the positive (lower) end of BL_3 extended by approximately 380 m relative to its position in Figure 5d. It is unknown whether this extension occurred before or after the negative (upper) end of BL_3 connected to the horizontal channel aloft. No further extension is seen in Figure 5f. The overall length of the negative end of BL_3 was approximately 730 m (see Figure 5f), which is almost the same as that of the positive end (approximately 720 m).

Figures 5g-5j show 4 consecutive images of BL_4, which occurred approximately 4.5 ms after BL_3. The initial height of BL_4 (3.35 km AGL and 250 m below the horizontal channel) was higher than those of BL_1 and BL_3. BL_4 extended bidirectionally along the decayed channel of BL_3 (see Figures 5h and 5i), and within approximately 20 μs the negative end of BL_4 connected to the horizontal channel (see Figure 5i). The brightness of BL_4 and the left part of the horizontal channel (to the left of the junction point) increased. Due to the positive end of BL_4 extending beyond the lower edge of Figure 5j, we couldn't obtain the total length of the positive end of BL_4 from Figure 5j. According to Figure 3h, the overall length of BL_4 channel was approximately 1820 m. The total length of the negative (upper) end of BL_4 was approximately 230 m (see Figure 5i), which is considerably shorter than that of its positive (lower) end (approximately 1590 m).

Like BL_1, BL_4 elongated abruptly (beyond the lower edge of Figure 5i) at the time of its connection to the horizontal channel (see Figures 5i and 5j). The abrupt elongation was by approximately 1070 m, as seen in Figure 3h, with a 2-D speed of approximately 5.4×10^7 m/s. Note that, similar to BL_2, the lower (positive) end of BL_4 channel was branched (see Figure 5j), which indicates that it extended into virgin air.

343

Figure 6. The 2-D speeds of negative and positive ends of the first bidirectional leader (BL$_1$), the third bidirectional leader (BL$_3$), and the fourth bidirectional leader (BL$_4$), based on the consecutive frames shown in Figure 4 (BL$_1$, HC-1) and Figure 5 (BL$_3$ and BL$_4$, HC-2). The red box and red circle at t = -20.43 ms represent the speeds of negative and positive ends, respectively, for the case if BL$_1$ was repolarized.

348   We estimated 2-D speeds of the positive and negative ends of BL_1, BL_3 and BL_4, based

349   on the consecutive frames of HC-1 and HC-2 (Figures 4a-4h, 5a-5f, and 5g-5j). Speed profiles

350   for the three bidirectional leaders (BL_1, BL_3, and BL_4) are shown in Figure 6. The 2-D nonzero

351   speeds of the negative and positive ends ranged from 1.4×10^6 to 1.2×10^7 m/s and from 9.5×10^5

352   to 1.9×10^7 m/s, respectively. The average (mean) speeds of the negative and positive ends were

353   approximately 6.5×10^6 m/s and 8.2×10^6 m/s, respectively. Note that the speeds for the first

354   leader (BL_1) are considerably lower than those for the subsequent leaders (BL_3 and BL_4). The

355   average (mean) extension speed of BL-formed downward branches after the negative BL end

356   connected to the horizontal channel was approximately 3.2×10^7 m/s.

357   We now present transient streamer-like discharges from the lateral surface of the

358   horizontal channel during the return-stroke later stage and the following continuing current.

359   Figure 7 shows a composite image of 480 selected HC-2 (20-μs interframe interval) frames for

360   the time interval of 0.4 to 10 ms (all after the +CG return-stroke onset). One can see 36 side

361   branches, labeled 1 through 36, extending primarily up and down (radially) from the horizontal

362   channel when the negative charge associated with the return-stroke later stage and the

363   following continuing current was injected into the horizontal channel core, probably

364   surrounded by a positive space charge sheath. These branches are numbered in the order of

365   their occurrence relative to the return stroke onset. Their time of occurrence is color coded.

366   Because these transient events were relatively far from the observation station, they produced

367   no detectable electric field changes (see FA and SA traces in Figure 2b). These branches appear

368   to be streamer filaments originating from the lateral surface of the horizontal channel, since

369   they are noticeably fainter and thinner than their parent channel.

370   These side branches were transient; that is, they decayed soon after extending from the

371   horizontal channel. Then some of the decayed (non-luminous) side branches were

372   reilluminated by one or more recoil leader or streamer type events. At the same time, some new

373   side branches were extending from other parts of the horizontal channel. Therefore, the

374   branches seen in Figure 7 are the cumulative effect of their formation process and

375   reillumination by the recoil type processes. Note that the recoil events caused the flickering of
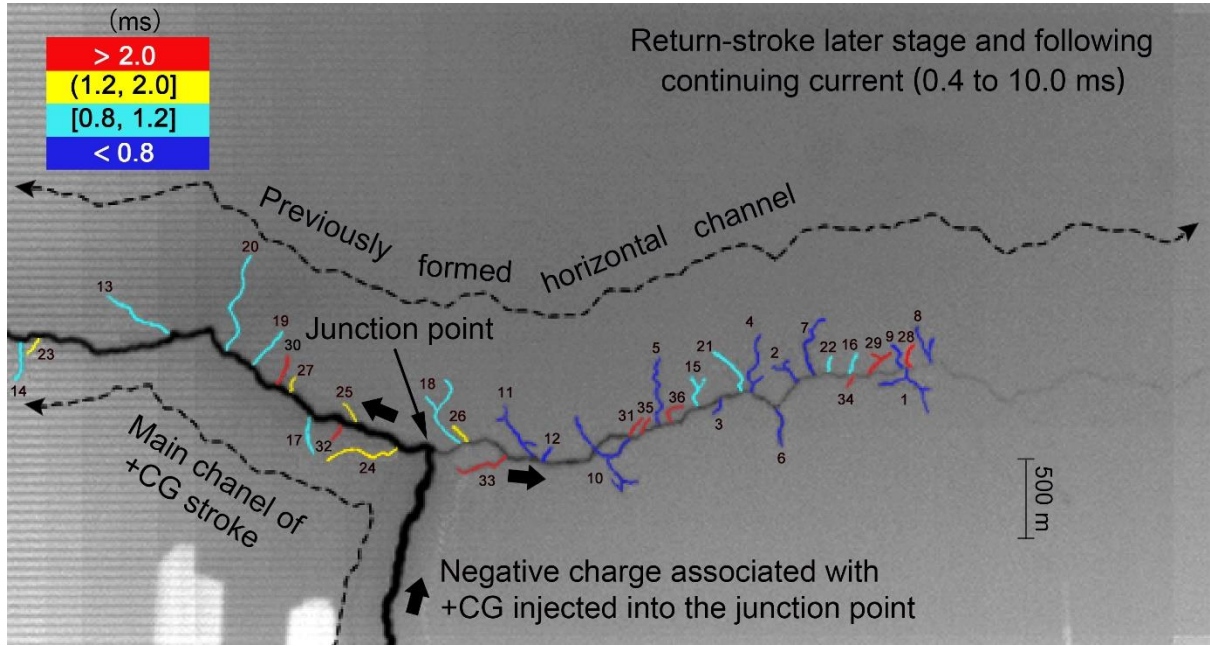
376   side branches.

Figure 7. Composite image of 480 selected frames (from 0.4 to 10.0 ms) obtained using HC-2 (20-μs interframe interval) showing side branches (different colors indicate their occurrence time relative to the RS onset) originating from the horizontal channel during the return-stroke later stage and continuing current. The composite image was inverted and contrast enhanced. Thick arrows indicate the direction of motion of negative charge associated with the +CG return stroke and continuing current along the vertical and horizontal channels. Discernible side branches (streamer-like filaments) are numbered 1 to 36 in the order of their occurrence relative to the RS onset.

Characteristics of the 36 streamer-like filaments including time intervals relative to the preceding one, 2D lengths, and 2-D extension speeds, are given in Table 1. We calculated the time interval between consecutive side branches as the interval between the time corresponding to the first image of a given side branch and that of the preceding one. It is unknown whether the channel seen in the first frame (0.40 ms) of #1 is true first image or one of its subsequent flickerings, due to the overexposure of the images caused by the +CG return stroke. For this reason, we do not give the initiation time and 2D extension speed of #1 in Table 1. The side (more or less radial) branches were observed within 0.4 to 10 ms of the onset of +CG return stroke and extended away from the horizontal channel over approximately 110

19

395   to 740 m (mean = 290 m) at speeds of approximately 5.0 to 19×10^6 m/s (mean = 9.6×10^6 m/s).

396   The time intervals between the side branches ranged from 0 to 2.32 ms (mean = 250 μs).

397   It is unknown whether similar streamer-like filaments occurred before 0.4 ms due to

398   overexposure of the images caused by the +CG return stroke. Before 0.8 ms, streamer-like

399   filaments appeared only on the right part of the horizontal channel. From 0.8 to 1.2 ms,

400   streamer-like filaments appeared on both the left and right parts of the horizontal channel.

401   From 1.2 to 2.0 ms, streamer-like filaments, except for #26 appeared only on the left part of

402   the horizontal channel. After 2.0 ms, streamer-like filaments, except for #30 and #32

403   appeared only on the right part of the horizontal channel. No new streamer-like filaments

404   were identified after 9.0 ms (see the second column in Table 1).

405   Note that both the left and the right parts of the horizontal channel increased in

406   brightness at the return stroke onset, even though the left part was always brighter. This

407   suggests that both the left and the right parts of the horizontal channel contributed to

408   supplying positive charge to the junction point (or, equivalently, the negative charge injected

409   by +CG into the junction point moved both to the left and to the right along the horizontal

410   channel). The hot (luminous) core of the horizontal channel was probably surrounded by a

411   non-luminous positive space charge sheath, formed during the +CG leader stage. Negative

412   charges pumped into the horizontal channel by the +CG return stroke and continuing current

413   were probably the cause of side branches (negative breakdowns) developing into and beyond

414   the positive space charge sheath.

415   Distributions of time intervals between the 36 side branches and their 2-D extension

416   speeds are shown in Figure 8. Minimum and maximum time intervals are 0 and 2.32 ms,

417   respectively, with a mean value of 250 μs. Most of the intervals (~62%) are shorter than 100

418   μs and ~85% are shorter than 300 μs. In many cases multiple events occurred simultaneously

419   or almost simultaneously (see the second column in Table 1). The minimum and maximum

420   extension speeds are 5×10^6 and 18.5×10^6 m/s, respectively, with a mean value of 9.6×10^6

421   m/s. In most (60%) of cases, the speed is lower than 10^7 m/s.

Table 1. Characteristics of 36 flickering side branches shown in Figure 7

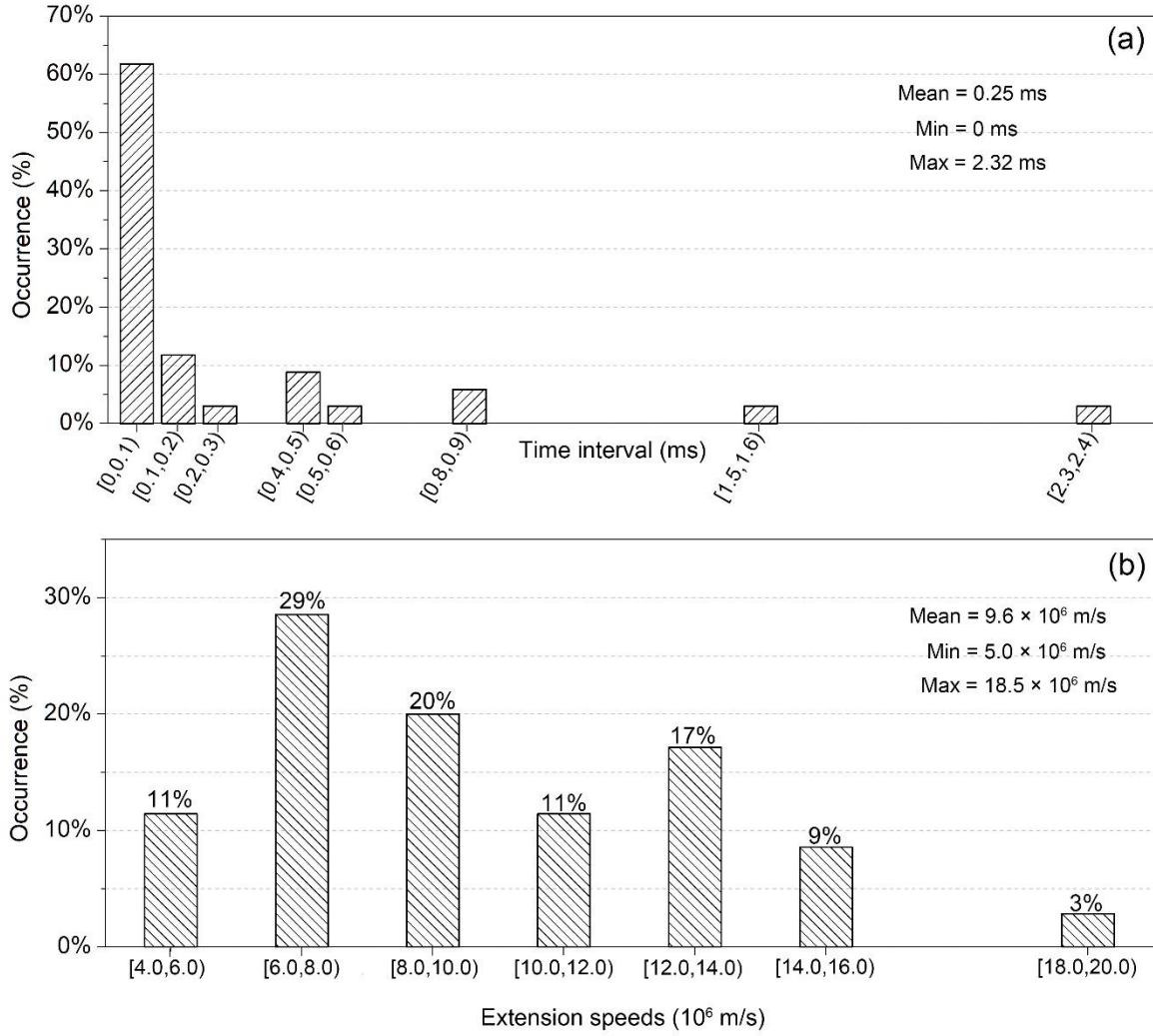| Side branch ID	Initiation time relative to RS onset (ms)	Initiation time relative to the preceding side branch (µs)	2D length (m)	2D extension speeds (10^6 m/s)
1		-	270	-
2	0.5	-	230	11.5
3	0.52	20	140	7.0
4	0.52	0	420	10.5
5	0.54	20	530	13.3
6	0.56	20	300	15.0
7	0.58	20	500	12.5
8	0.58	0	280	7.0
9	0.62	40	200	10.0
10	0.64	20	580	14.5
11	0.68	40	390	9.8
12	0.7	20	120	6.0
13	0.8	100	530	13.3
14	0.84	40	270	13.5
15	0.84	0	230	11.5
16	0.84	0	150	7.5
17	0.86	20	270	13.5
18	0.9	40	560	14.0
19	0.9	0	320	8.0
20	0.92	20	740	18.5
21	0.96	40	370	9.3
22	1.2	240	120	6.0
23	1.24	40	130	6.5
24	1.34	100	550	13.8
25	1.88	540	170	8.5
26	2	120	150	7.5
27	2	0	110	5.5
28	2.4	400	200	5.0
29	4.72	2320	220	5.5
30	5.56	840	220	5.5
31	5.98	420	160	8.0
32	6.1	120	130	6.5
33	6.54	440	390	9.8
34	6.6	60	120	6.0
35	7.44	840	140	7.0
36	9	1560	190	9.5
Mean	-	250	290	9.6

Figure 8. (a) Distribution of time intervals and (b) 2D extension speeds of 36 side branches (see also Table 1).

4. Discussion and Summary

A sequence of four bidirectional leaders (BL_1-BL_4) served to form a new positive branch originating from the previously formed horizontal channel aloft and eventually attached to the ground and initiated a 135-kA +CG return stroke. To the best of our knowledge, this is the most detailed study of the process of formation of in-cloud channel branch that extended toward ground and caused +CG to date. Additionally, we observed negative streamer-like filaments extending sideways from the positively charged horizontal channel in response to the injection of negative charge associated with the +CG.

On a possible background discharge prior to BL_1. Our optical records (including LCI images and high-speed video camera images) show that there were no positive leader or

22

436   streamer-like branches emanating from the predominantly horizontal channel before BL_1,

437   probably due to (1) not long enough recording time (-25 to 25 ms) of high-speed cameras

438   operating at 20, 000 frames per second, (2) insufficient temporal resolution (~20 ms) of LCI

439   having a longer recording time (2 s), or (3) very low brightness of positive leader or streamer

440   branches within the visible wavelength range (380 to 780 nm) of our cameras.

441   The 2D extension speeds of negative and positive ends of BL_1 ranged from 9.5×10^5 to

442   4×10^6 m/s (see Figure 6), which is near the upper bound or higher than the average extension

443   speed of leaders in virgin air (~10^4 to 10^6 m/s). Such relatively higher extension speeds at the

444   positive and negative ends of BL_1 seem to suggest that BL_1 may have initiated and developed

445   in the previously created but optically undetectable channel.

446   At the same time, we cannot rule out a possibility that there were no positive

447   leader/streamer branches emanating from the predominantly horizontal channel or

448   bidirectional leaders before BL_1, because (a) leaders in virgin air are known (e.g., Berger and

449   Vogelsanger, (1969); Orville and Idone, (1982); Chen et al., 1999; Lu et al., (2008)) to be able

450   to propagate at speeds of the order of 10^6 m/s and (b) extension speeds for BL_3 and BL_4 in our

451   study are considerably higher than those for BL_1 (see Figure 6).

452   **Initiation of vertical bidirectional leaders.**   It is known (e.g., Maslowski and

453   Rakov, 2006) that the bulk of leader charge is contained in the corona (space charge) sheath

454   formed around the narrow hot core. Therefore, the horizontal channel seen in our high-speed

455   video camera images is a narrow hot core surrounded by optically undetectable corona

456   sheath, whose outer radius should be up to tens of meters (e.g., for leader line charge density

457   of 1 mC/m, the corona-sheath radius should be about 20 m, according to Gauss Law). The

458   horizontal channel was positive at the time of BL_1-BL_4. The shielding effect of the positive

459   corona sheath around the positive hot core should suppress the development of branches

460   directly from the core. For this reason, such branches are more likely to be formed via

461   bidirectional leaders excited outside the positive corona sheath. BL_1 to BL_4 initiated at

462   distances of approximatively 250 to 700 m from the luminous horizontal channel, from which

463   we infer that the radius of the positive corona sheath was less than 250 m. It is worth noting

464   that the radius of corona sheath for positive polarity is expected to be greater than that for

465 negative polarity (because of the lower propagation field threshold for positive streamers) and

466 that the initiation point of later BLs should have been influenced by the presence of remnants

467 of preceding BLs.

468 **Dynamics of bidirectional leaders.** We start with a brief overview of the literature

469 on bidirectional leaders making connection to positively charged channels. Most of the time,

470 bidirectional leaders are completely or in part hidden inside the cloud, which makes their

471 optical imaging impossible. Therefore, as of today, there are only a few optical observations

472 of bidirectional leaders found in the literature. Montanya et al. (2015) and Warner et al.

473 (2016) reported on bidirectional leaders making connection to pre-existing positively charged

474 channels of cloud and ground lightning discharges, respectively. Further, Pilkey (2014,

475 Figures. A-1 and A-2) reported on a floating channel segment that initiated about 84 m from

476 the positive in-cloud leader channel near 3-km altitude and 364 μs later connected to the

477 lateral surface of that channel. Tran and Rakov (2016), using a high-speed video camera,

478 observed a natural lightning discharge that started with a bidirectional leader. The negative

479 end of the bidirectional leader extended toward the ground (and eventually produced a return

480 stroke), while its positive end, developing primarily horizontally, exhibited an abrupt

481 extension that was relatively straight and had a 2-D length of about 1 km. Tran and Rakov

482 (2016) tentatively interpreted this event as a gigantic, kilometer-scale positive-leader step that

483 developed from a space stem/leader and connected to the lateral surface of the existing

484 positive channel, creating a major positive branch. This newly-created branch faded and then

485 was re-illuminated four times with a remarkably constant time interval of 1.2 ms. The rate at

486 which the new positive branch was formed was at least 1.6×10^6 m/s if it originated from the

487 mid-point of the newly-formed branch. Additionally, Pu and Cummer (2019), who used a

488 100-200 MHz broadband interferometer, observed a bidirectional leader that initiated

489 approximately 500 m from a positive in-cloud channel and whose negative end connected to

490 the positive channel.

491 In this study, the formation of a new downward positive branch was facilitated by

492 four bidirectional leaders sequentially retracing the same path. The resultant downward

493 branch elongated abruptly at the time of negative end of BL_1 and BL_4 connected to the

494 floating horizontal channel (see Figures 4f and 5j). Some elongation of the positive ends of

495 BLs prior to connection could have occurred in the same frame. The lengths of abrupt

496 elongations of new branches were obtained by comparing the tip positions in the connection

497 frame and in the frame immediately after connection (see Figures 4e and 4f; Figures 5i, 5j,

498 and 3h). The abrupt extension events exhibited some similarities with the so-called restrike

499 phenomenon reported by Les Renardieres Group (1972, 1977) from long positive laboratory

500 spark experiments. However, the 2-D speeds of the abrupt extensions (BL_1, approximately

501 1.1×10^7 m/s in virgin air; BL_4, approximately 5.4×10^7 m/s along the remnants of BL_3 and

502 extended into virgin air, unless there was an optically undetectable channel prior to BL_1)

503 were much higher than the long-spark restrike speeds (0.5 to 2.0×10^5 m/s) based on the

504 observations of Chen et al. (2016). The abrupt extension lengths (approximately 530 and

505 1070 m) were much larger than the abrupt extensions of the positive end of a subsequent

506 leader (approximately 91 to 160 m) reported by Wu et al. (2019a), but were comparable to

507 that of the 1‑km‑long extension occurring at the positive end of the bidirectional leader

508 observed by Tran and Rakov (2016).

509 **Side branches from the lateral surface of the horizontal channel in response to**

510 **+CG.**   Before the +CG return stroke, the vertical and horizontal channels each consisted of

511 a narrow hot core surrounded by an optically undetectable radial corona sheath containing the

512 positive space charge deposited there by the leader. The 135-kA +CG return stroke

513 effectively transported negative charge toward the junction point and into the horizontal

514 channel, to neutralize the positive leader charge. The negative charge (some tens of coulombs

515 expected for the 135-kA peak current) rapidly injected into the horizontal-channel hot core

516 caused negative breakdown, in the form of side branches, into the positive corona sheath

517 surrounding the hot core. The side branches extended over roughly 110 to 740 m with a mean

518 of 290 m (probably beyond the positive corona sheath, which is expected to have radial

519 dimension up to tens of meters) at speeds ranging from ~0.5 to 1.9×10^7 m/s with a mean of

520 9.6×10^6 m/s and exhibited flickering. It is likely that the side branches are the most intense

521 (thermalized) streamers of the so-called reverse corona discussed in detail by Maslowski and

522 Rakov (2006, 2009).

523   In some respects the side branches are similar to the recently discovered "needles"

524 observed via RF channel imaging by Hare et al. (2019) and Pu and Cummer (2019) and

525 optically by Saba et al. (2020). The similarities include (1) the extension from the lateral

526 surface of positively charged channels, (2) lengths of the order of 10 to 100 m (from 30 to

527 100 m in Hare et al. (2019), 60 m in Pu and Cummer (2019), and from 2.3 to 73 m (mean =

528 14.3 m) in Saba et al. (2020); in our case a little longer), and (3) flickering. On the other hand,

529 extension speeds are different: 10^5 to 10^6 m/s for "needles" (3×10^5 m/s in Hare et al., (2019),

530 $1\text{-}10 \times 10^5$ m/s in Pu and Cummer (2019), and 2.7×10^5 m/s (on average, 2D) in Saba et al.

531 (2020)) vs. 10^6 to 10^7 m/s for our side branches. Also, "needles" flicker at time intervals of

532 some milliseconds (from 3 to 7 ms in Hare et al. (2019), from 6 to 7 ms in Pu and Cummer

533 (2019), and from 0.3 to 34 ms (mean = 2.6 ms) in Saba et al. (2020)), while our side branches

534 flicker at intervals of a factor of 10 to 100 shorter (mean = 0.1 ms). Thus, our side branches

535 extend faster and flicker at a higher rate. The reason for the difference in the extension speed

536 and flickering rate between our side branches and the "needles" may be that the

537 135-kA-return-stroke later stage and the following continuing current of our +CG flash

538 injected a considerably large negative charge (tens of coulombs are expected) into the positive

539 horizontal channel than charges associated with in-cloud positive leaders studied by Hare et al.

540 (2019) and Pu and Cummer (2019) or upward positive leaders developing from grounded

541 objects reported by Saba et al. (2020). Positive leader currents in upward and rocket-and-wire

542 triggered lightning are of the order of 100 A (Miki et al., (2005)), about 2 orders of

543 magnitude lower than continuing currents following return strokes in +CG flashes (Rakov

544 and Uman, 2003, p.222). Of course, the two phenomena occur in different contexts (leader

545 vs. return stroke), but their physics should be similar. In our future work, we will quantify the

546 characteristics of side branches in more detail and compare more parameters of streamer-like

547 filaments observed in this study (see also Wu et al., (2020) published in ESSOAR) and

548 needle-like structures reported by Hare et al., (2019), Pu and Cummer, (2019), and Saba et

549 al., (2020).

References

Berger, K., and E. Vogelsanger (1969), New results of lightning observations, in Planetary Electrodynamics, edited by S. C. Coroniti and J. Hughes, pp. 489–510, Gordon and Breach, New York.

Chen M, Takagi N, Watanabe T, Wang D, Kawasaki Z, and Liu X. (1999). Spatial and temporal properties of optical radiation produced by stepped leaders. Journal of Geophysical Research, 104: 27573-27584. http://doi: 10.1029/1999JD900846

Chen, S., Zeng, R., Zhuang, C., Zhou, X. and Ding, Y. (2016). Experimental study on branch and diffuse type of streamers in leader restrike of long air gap discharge. Plasma Sci. Technol. 18, 305–310. http://doi: 10.1088/1009-0630/18/3/15

Hare, B. M., Scholten, O., Dwyer, J., Trinh, T. N. G., Buitink, S., ter Veen, S., et al. (2019). Needlelike structures discovered on positively charged lightning branches. Nature, 568(7752), 360–363. https://doi.org/10.1038/s41586-019-1086-6

Jiang, R., Wu, Z., Qie, X., Wang, D., and Liu, M. (2014). High-speed video evidence of a dart leader with bidirectional development. Geophysical Research Letters, 41, 5246–5250. https://doi.org/10.1002/ 2014GL060585

Kong, X., X. Qie, and Y. Zhao (2008), Characteristics of downward leader in a positive cloud-to-ground lightning flash observed by high-speed video camera and electric field changes, Geophysical Research Letters, 35, L05816. http://doi:10.1029/2007GL032764

576 Kostinskiy, A. Yu, V. S. Syssoev, N. A. Bogatov, E. A. Mareev, M. G. Andreev, L. M.

577 Makalsky, D. I. Sukharevsky, and V. A. Rakov (2015), Infrared images of bidirectional

578 leaders produced by the cloud of charged water droplets, Journal of Geophysical

579 Research: Atmospheres, 120, 10,728–10,735. http://doi:10.1002/2015JD023827

580 Les Renardieres Group (1972). Research on long air gap discharges at Les Renardieres. Electra

581 23, 53–157.

582 Les Renardieres Group (1977). Positive discharges in long air gaps at Les Renardieres, 1975

583 results and conclusions. Electra 53, 31–153.

584 Lu, W., D. Wang, N. Takagi, V. Rakov, M. Uman, and M. Miki (2008), Characteristics of the

585 optical pulses associated with a downward branched stepped leader, Journal of

586 Geophysical Research: Atmospheres, 113, D21206. http://doi:10.1029/2008JD010231

587 Lu, W., L. Chen, Y. Zhang, Y. Ma, Y. Gao, Q. Yin, S. Chen, Z. Huang, and Y. Zhang (2012),

588 Characteristics of unconnected upward leaders initiated from tall structures observed in

589 Guangzhou, Journal of Geophysical Research: Atmospheres, 117, D19211.

590 http://doi:10.1029/2012JD018035

591 Lu, W., L. Chen, Y. Ma, V. A. Rakov, Y. Gao, Y. Zhang, Q. Yin, and Y. Zhang (2013),

592 Lightning attachment process involving connection of the downward negative leader to

593 the lateral surface of the upward connecting leader, Geophysical Research Letters, 40,

594 5531-5535. http://doi:10.1002/2013GL058060

595 Maslowski, G., and Rakov, V. A. (2006). A study of the lightning channel corona sheath.

596 Journal of Geophysical Research Atmospheres, 111(D14).

597 https://doi.org/10.1029/2005JD006858

598 Maslowski, G. and Rakov, V.A. (2009). New insights into lightning return-stroke models with

599 specified longitudinal current distribution. IEEE Transactions on Electromagnetic

600 Compatibility, 51(3), 471-478. https:// doi:10.1109/TEMC.2009.2017200

601 Miki, M., V. A. Rakov, T. Shindo, G. Diendorfer, M. Mair, F. Heidler, W. Zischank, M. A.

602 Uman, R. Thottappillil, and D. Wang (2005), Initial stage in lightning initiated from tall

603   objects and in rocket-triggered lightning, J. Geophys. Res., 110, D02109.

604   https://doi:10.1029/2003JD004474.

605 Montanyà, J., van der Velde, O., and Williams, E. R. (2015). The start of lightning: Evidence of

606   bidirectional lightning initiation. Scientific Reports, 5, 15180.

607   https://doi.org/10.1038/srep15180

608 Nag, A., and Rakov, V. A. (2012). Positive lightning: an overview, new observations, and

609   inferences. Journal of Geophysical Research: Atmospheres, 117(D8).

610   https://doi.org/10.1029/2012JD017545

611 Orville, R. E., and V. P. Idone, Lightning leader characteristics in the Thunderstorm Research

612   International Program (TRIP), (1982). Journal of Geophysical Research, 87,

613   11,177-11,192. https://doi:10.1029/JC087iC13p11177

614 Pilkey, J. T. (2014). The physics of lightning studied using lightning mapping array, electric

615   field, and optical measurements, PhD dissertation, University of Florida.

616 Pu Y. and Cummer S. A. (2019). Needles and Lightning Leader Dynamics Imaged with 100–

617   200 MHz Broadband VHF Interferometry. Geophysical Research Letters, 46(22).

618   http://doi: 10.1029/2019gl085635

619 Qi, Q., Lyu, W., Wu, B., Ma, Y., Chen, L., and Liu, H. (2018). Three-dimensional optical

620   observations of an upward lightning triggered by positive cloud-to-ground lightning.

621   Atmospheric Research, 214, 275-283. http://doi:10.1016/j.atmosres.2018.08.003

622 Rakov, V. A., Uman, M. A., Rambo, K. J, Fernandez, M. I., Fisher, R. J., and Schnetzer, G. H.,

623   et al. (1998). New insights into lightning processes gained from triggered-lightning

624   experiments in Florida and Alabama. Journal of Geophysical Research, 103(D12),

625   14117, http://doi:10.1029/97JD02149

626 Rakov, V. A., and M. A. Uman (2003). Lightning: Physics and Effects, Cambridge Univ.

627   Press, New York.

628 Saba, M. M. F., K. L. Cummins, T. A. Warner, E. P. Krider, L. Z. S. Campos, M. G. Ballarotti,

629   O. Pinto Jr., and S. A. Fleenor (2008), Positive leader characteristics from high-speed

630   video observations, Geophysical Research Letters, 35, L07802.

631   http://doi:10.1029/2007GL033000

632 Saba, M. M. F., L. Z. S. Campos, E. P. Krider, and O. Pinto Jr. (2009). High-speed video

633   observations of positive ground flashes produced by intracloud lightning, Geophysical

634   Research Letters, 36, L12811. http://doi:10.1029/2009GL038791

635 Saba, M. M. F., Paiva, A. R. D., Concollato, L. C., Warner, T. A., and Schumann, C. (2020).

636   Optical observation of needles in upward lightning flashes. Scientific Reports, 41598.

637   https://doi.org/10.1038/s41598-020-74597-6

638 Shao, X., C. T. Rhodes, and D. N. Holden (1999), RF radiation observations of positive

639   cloud-to-ground flashes, Journal of Geophysical Research, 104(D8), 9601-9608.

640   http://doi:10.1029/1999jd900036

641 Takamatsu, K. Takagi, N. and Wang D. (2015). Characteristics of the brief but bright

642   discharges that often occur along the trails of positive leaders. Journal of Atmospheric

643   Electricity. 35, 17-30. https://doi.org/10.1541/jae.35.17

644 Tran, M. D., and Rakov, V. A. (2016). Initiation and propagation of cloud-to-ground lightning

645   observed with a high-speed video camera. Scientific Reports, 6, 39521.

646   http://doi:10.1038/srep39521

647 Wang, D., Watanabe, T., and Takagi, N. (2011). A high speed optical imaging system for

648   studying lightning attachment process. 7th Asia-Pacific International Conference on

649   Lightning. https://doi.org/10.1109/apl.2011.6111050

650 Warner, T. A., Saba, M. M. F., Schumann, C., Helsdon, J. H. and Orville, R. E (2016).

651   Observations of bidirectional lightning leader initiation and development near positive

652   leader channels. Journal of Geophysical Research: Atmospheres, 121, 9251-9260.

653   http://doi: 10.1002/2016JD025365

654 Wu, B., Lyu, W., Qi, Q., Ma, Y., Chen, L., Jiang, R., Zhu, Y. and Rakov, V. A. (2019a). High-

655   speed video observations of recoil leaders producing and not producing return strokes

656   in a Canton-Tower upward flash. Geophysical Research Letters, 46, 8546–8553.

657   http://doi:10.1029/2019GL083862

658 Wu, B., Lyu, W., Qi, Q., Ma, Y., Chen, L., Zhang, Y., Zhu, Y. and Rakov, V. A. (2019b).

659   Synchronized two-station optical and electric field observations of multiple upward

660   lightning flashes triggered by a 310 kA +CG flash. Journal of Geophysical Research:

661   Atmospheres, 124, 1050–1063. https://doi.org/10.1029/2018JD02937

662 Wu, B., Lyu, W., Qi, Q., Ma, Y., Chen, L., Jiang, R., Zhu, Y. and Rakov, V. A. (2020). A +CG

663   flash caused by a sequence of bidirectional leaders that served to form a

664   ground-reaching branch of a pre-existing horizontal channel. Preprint published in

665   ESSOAR on Aug. 11. https://doi:10.1002/essoar.10503631.1

666 Yuan, S., Jiang, R., Qie, X., Sun, Z., Wang, D., and Srivastava, A., (2018). Development of

667   side bidirectional leader and its effect on channel branching of the progressing positive

668   leader of lightning. Geophysical Research Letters, 46, 1746-1753.

669   http://doi:10.1029/2018GL080718